An Improved United Atom Force Field for Simulation of Mixed Lipid Bilayers

See-Wing Chiu,[†] Sagar A. Pandit,[‡] H. L. Scott,*[,§] and Eric Jakobsson[†]

Department of Molecular and Integrative Physiology, Department of Biochemistry, UIUC Programs in Biophysics, Neuroscience, and Bioengineering, National Center for Supercomputing Applications, and Beckman Institute, University of Illinois, Urbana, Illinois 61801, Department of Physics, University of South Florida, Tampa, Florida 33620, and Department of Biological, Chemical, and Physical Science, Illinois Institute of Technology, Chicago, Illinois 60616

Received: August 7, 2008; Revised Manuscript Received: December 5, 2008

We introduce a new force field (43A1-S3) for simulation of membranes by the Gromacs simulation package. Construction of the force fields is by standard methods of electronic structure computations for bond parameters and charge distribution and specific volumes and heats of vaporization for small-molecule components of the larger lipid molecules for van der Waals parameters. Some parameters from the earlier 43A1 force field are found to be correct in the context of these calculations, while others are modified. The validity of the force fields is demonstrated by correct replication of X-ray form factors and NMR order parameters over a wide range of membrane compositions in semi-isotropic NTP 1 atm simulations. 43-A1-S3 compares favorably with other force fields used in conjunction with the Gromacs simulation package with respect to the breadth of phenomena that it accurately reproduces.

1. Introduction

The successful application of molecular dynamics (MD) simulation to lipid bilayers and other complex molecular systems is dependent upon accurate sets of interaction parameters (force fields). As more complex lipids, lipid mixtures, and membrane peptides and proteins are studied by simulation, force field parameters must be updated and improved. The details of the force field depend on whether all hydrogen atoms are to be included in the simulation (all-atom) or whether hydrogen atoms on the nonpolar molecules (methylenes and terminal methyls) are replaced by effective van der Waals spheres (united atom). For all-atom force fields, the most widely used force fields are included in the CHARMM simulation code package. In this paper, we will address only united atom force fields.

Current force fields that are used widely in united atom simulations are largely based on the GROMACS 43A1 force field.[1,12] This force field, in turn, evolved from earlier force fields designed by developers of the GROMOS molecular modeling software package.[22] In 1997, Berger et al.[2] improved the hydrocarbon chain parameters by fitting MD simulations of liquid pentadecane to molecular volume and heat of vaporization experimental data. This effort was further improved by Chiu et al.,[4] who fit hydrocarbon chain simulations of hexane, decane, and pentadecane simultaneously to experimental volumes and heats of vaporization. For the polar head group of the most commonly studied phospholipids, dipalmitoyl phosphatidylcholine (DPPC) and dimyristoyl phosphatidylcholine (DMPC), force field partial charges were calculated by Chiu et al.[3] and remain in use in most current united atom force fields. In a simulation study of sphingomyelin bilayers (SM),[5] the van der Waals parameters for hydrocarbon chains were recalculated by fitting simulation data to a newer and more comprehensive volume and heat of vaporization data set for hydrocarbon liquids. By using a greater variety of hydrocarbon liquids as targets, they constructed a comprehensive set of force field parameters for the saturated and unsaturated hydrocarbon chains of PC and cholesterol.

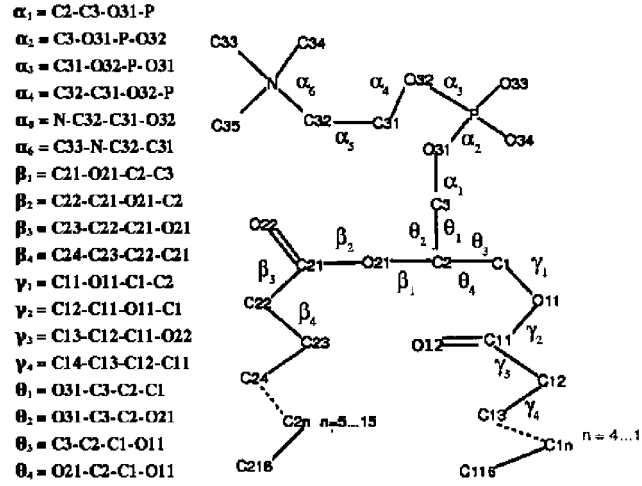

Figure 1. Figure 1. Molecular topolgy and labeling scheme for a united atom DPPC molecule.

In all prior united-atom-based force field updates, the torsional parameters for the polar head group were taken from the original GROMOS96 force fields. However, for a given force field, use of different partial charges can lead directly to changes in the landscapes of torsional energy profiles for the individual dihedral angles of the polar head group. This, in turn, causes improper sampling of allowed conformations in a MD simulation. To be consistent with the use of the charge set of Chiu et al.[3] for lipid bilayer simulations, we have now re-evaluated the torsional parameters for the PC head group guided by the ab initio torsional profiles.

The parametrization results described in this paper have their origin in the GROMOS96 43A1 parameter set.[22] Combined with

* To whom correspondence should be addressed.
[†] University of Illinois.
[‡] University of South Florida.
[§] Illinois Institute of Technology.

10.1021/jp807056c CCC: $40.75
Published on Web 02/09/2009

TABLE 1: Comparison of the *n*-Alkane Lennard-Jones parameters for the OPLS,[37] TraPPE,[38] NERD,[39] 53a6,[40] and 43A1-S3 Force Fields[a]

	OPLS		TraPPE		NERD		53A6		43A1-S3	
atom	ε/k_B (K)	σ(Å)	ε/k_B (K)	σ (Å)	ε/k_B (K)	σ (Å)	ε/k_B (K)	σ (Å)	ε/k_B (K)	σ (Å)
CH3	88.1	3.905	98	3.750	104	3.91	104.3	3.747	98.6	3.750
CH2	59.400	3.905	46	3.95	45.8	3.91	49.4	4.070	48.6	4.077

[a] The 53A6 alkane force field parameters are derived from the GROMOS 45A3 parameter set.[41]

TABLE 2: Atom Labels, Types, And Charges (in units of e^-) for DPPC

atom label[a]	atom type	description	charge
C33, C34, C35	CH3*	choline methyl group	0.4
N	NL	choline nitrogen	−0.5
C32	CH2*	aliphatic methylene group	0.3
C31	CH2*	aliphatic methylene group	0.4
O32	OA	phosphate ester oxygen	−0.8
P	P	phosphorus	1.7
O33, O34	OM*	phosphate oxygen	−0.8
O31	OA	phosphate ester oxygen	−0.7
C3	CH2*	aliphatic methylene group	0.4
C2	CH1*	aliphatic methylidyne group	0.3
C1	CH2*	aliphatic methylene group	0.5
O11, O21	OA	ester oxygen	−0.7
C11	CO*	carbonyl carbon	0.8
O12	O*	carbonyl oxygen	−0.6
C21	CO*	carbonyl carbon	0.7
O22	O*	carbonyl oxygen	−0.7
C12, C13,..., C115	CH2*	aliphatic methylene group	0.0
C22, C23,..., C215	CH2*	aliphatic methylene group	0.0
C116, C216	CH3*	aliphatic methyl group	0.0
OW	OW	water oxygen	−0.8476
HW1, HW2	H	water hydrogen	0.4238

[a] Refer to Figure 1 for atom labels.

our recent force field developed for SM,[5] we describe here a comprehensive and consistent force field for PC/SM/cholesterol MD simulations. We have validated this parameter set, which we call 43A1-S3, by MD simulations that replicate experimental structures of bilayers,[24,25] including X-ray form factors, electron densities, order parameters, and molecular volumes. In this paper, we present our parametrization results and compare our simulation results for saturated PCs, dilauryl phosphatidylcholine (DLPC), DMPC, and DPPC with the experimental structures of these fluid-phase bilayers. We have also applied the 43A1-S3 parameter set to MD simulations for monounsaturated PC bilayers (DOPC and POPC) as well as DPPC bilayers, including pure bilayers and bilayers with cholesterol.[15] This paper is organized as follows. The following section describes the methods and the model compounds used for the evaluation of force field parameters for different subunits of phospholipids. The Results section describes MD simulations of a number of hydrated lipid bilayers that were run to validate the chosen parameters. Table 2 lists the atom labels along with the previously determined partial charges. Parameter groups that were not altered in this work are identical to those in the GROMOS 96 43A1 set. The complete 43A1-S3 force field is available in GROMACS format as Supporting Information to this paper, and for download at www.nanoconductor.org/43A1-S3.

2. Methods Section

Here, we describe the various methods used to calculate the revised force field parameters. The results of the parametrization and results of MD tests of the parameters are given in the Results section and in Tables 3−8. All of the atom and united atom types in the 43A1-S3 force field presented in this paper are designated by the addition of the symbol * to the common Gromacs terminology. For example, CH2 becomes CH2*. For those groups that may be either in a completely saturated or partly unsaturated bond environment, the two species of united atom are differentiated by the positioning of the *. If the bonding environment is completely saturated, the * is at the end, as in CH1*. If the bonding environment is partly unsaturated, the * comes after the first constituent individual atom, as in C*H1. Note that the *-ed united atoms are not presented as a complete substitute for all of the united atoms in 43A1 or other Gromacs force fields, but only as the ones we have found most suitable for lipids. Thus, if one does simulations involving both proteins and lipids, one might use 43A1-S3 for the lipids and a standard Gromacs force field for the proteins.

In constructing self-consistent force fields, one is faced with a "chicken-and-egg" problem in the sense that one must assume given torsion angles to calculate van der Waals parameters and one must assume given van der Waals parameters to calculate torsion angle energy functions. Therefore, it was necessary to do successive iterations between van der Waals parametrization and torsion angle parametrization in order to finally arrive at a force field for both optimally replicated relevant experimental data. In the following text, we describe details of the individual components of this iterative process. The actual starting point was to reparameterize van der Waals parameters using previously existing torsion angle parameters. We then reparameterized the torsion angles with the new van der Waals parameters, revisited the van der Waals parametrization with the new torsion angles, and so forth.

TABLE 3: Normal ($C_6^{1/2}$, $C_{12}^{1/2}$) and 1−4 ($CS_6^{1/2}$, $CS_{12}^{1/2}$) van der Waals Parameters for (a) PC Lipid and SPC/E Water and (b) the Hydrocarbons Studied in This Work[a]

(a)

atom type	$C_6^{1/2}$ (I,I)	$C_{12}^{1/2}$ (I,I)			$CS_6^{1/2}$ (I,I)	$CS_{12}^{1/2}$ (I,I)
		1	2	3		
CH1*	5.7633	5.7518			2.2439	1.2317
CH2*	8.6103	5.8346			5.18	1.95
CH3*	9.5506	5.0364			5.75	2.035
C*H1	8.2384	4.916			5.74	1.71
NL	4.936	1.301	3.068		4.936	1.301
P	12.14	4.711			12.14	4.711
OA	4.756	1.125	1.227		4.756	1.125
OM*	4.756	1.125	1.841	3.068	4.756	8.611
O*	4.756	1.125	1.125		4.756	8.611
CO*	5.5579	5.187			1.965	1.3672
OW	5.116	1.544	1.623			
H	0.0	0.0			0.0	0.0

(b)

atom type	$C_6^{1/2}$ (I,I)	$C_{12}^{1/2}$ (I,I) 1	$CS_6^{1/2}$ (I,I)	$CS_{12}^{1/2}$ (I,I)	description
CH0*	5.05	14.25	4.838	1.837	SP3 bare carbon
CH1*	5.7633	5.7518	2.2439	1.2317	SP3 CH group
CH2*	8.6103	5.8346	5.18	1.95	SP3 CH_2 group
CH3*	9.5506	5.0364	5.75	2.035	SP3 CH_3 group
C*H1	8.2384	4.916	5.74	1.71	SP2 CH group
C*	5.5579	3.867	1.965	9.4293	SP2 bare carbon
CH1R5	5.5635	6.0518	2.2439	1.2317	SP3 CH in five-membered ring
CH2R5	9.1412	5.6586	5.18	1.95	SP3 CH_2 in five-membered ring
CH1R6	5.5635	6.1018	2.2439	1.2314	SP3 CH in six-membered ring
CH2R6	8.3594	5.1135	5.18	1.95	SP3 CH_2 in six-membered ring
C*HR6	8.2367	4.5041	5.75	1.77	SP2 CH_2 in six-membered ring

[a] $C_6^{1/2}$(I,I) and $CS_6^{1/2}$ (I,I) in 10^{-2} [kJ mol $^{-1}$ nm^6]$^{1/2}$. $C_{12}^{1/2}$ (I,I) and $CS_{12}^{1/2}$ (I,I) in 10^{-3} [kJ mol^{-1} nm^{12}]$^{1/2}$. Italic numbers are original 43A1 values.

TABLE 4: Force Field Parameters for the Bond Stretching Terms in (a) PC Lipids and (b) Cholesterol and Other Hydrocarbons

bond type (a)	force constant K_b (10^6 mol^{-1} nm^{-4})	ideal bond length (nm)
CH2*−CH3*, CH1*−CH2*	7.15	0.153
C*H1−C*H1	10.25	0.134
CH2*−C*H1	7.50	0.150
NL−CH2*, NL−CH3*	8.71	0.147
CH1*, CH2*−OA	8.18	0.143
P−OA	4.84	0.161
P−OM*	8.60	0.148
CO*−OA	10.20	0.136
CO*−O*	16.60	0.123
CO*−CH2*	7.15	0.152
(b)		
CH1R6−CH1R6, CH2R6−CH2R6	7.15	0.153
CH1R6−CH2R6, CH1R5−CH1*	7.15	0.153
CH0*−CH1R6, CH0*−CH2R6, CH1R5−CH1*	7.15	0.153
CH1*−CH2*, CH1*−CH3*, CH2*−CH2*	7.15	0.153
CH0*−CH3*	7.15	0.153
C*−C*HR6	10.25	0.134
CH2*−C*H1	7.50	0.150
C*−CH2R6, C*−CH0*, C*HR6−CH2R6	7.50	0.151
CH0*−CH1R5, CH1R6−CH2R5	7.15	0.154
CH2R5−CH2R5, CH1R5−CH2R5	7.15	0.154
CH1R6−OA	8.18	0.143
OA−H	15.70	0.100

The force field determination was generally done in a manner that determined the parameters for just one molecular group for each computation. For example, the parameters for methyl were determined by comparison with the physical properties

TABLE 5: Force Field Parameters for the Bond Angle Terms in PC Lipids, Cholesterol, and Hydrocarbons

bond angle type	force constant K_θ (kJ mol^{-1})	ideal bond angle (degree)
CHn*−CH2*−CHn*, n = 2, 3; CH3*−CH2*-CH1*	530	111.0
CH2*−CH2*−CH1*	530	111.0
CHn*−CH1*−CHn*, n = 2, 3	520	109.5
CH3*−CH1*−CH2*	520	109.5
CH3*−CH0*−CH0*, CH3*−CH0*−CH3*	520	109.5
CH2*−CH2*−CH3*, CH1*−CH2*−OA	530	111.0
CH2*−CH1*−OA	520	109.5
CH2*−CH2*−C*H1	530	112.0
C*H1−C*H1−CH2*	615	126.0
CHn*−OA−CO*, n = 1, 2	610	115.0
CH3*−NL−CH3*, CH3*−NL−CH2*	520	109.5
CH2*−CH2*−NL	530	111.0
CH2*−OA−P	530	120.0
CO*−CH2*−CH2*	530	111.0
O*−CO*−CH2*	750	125.0
OA−CH2*−CH2, NL−CH2*−CH2*	530	111.0
OA−CO*−O*	730	124.0
OA−CO*−CH2*	530	111.0
OA−P−OM*	450	109.5
OA−P−OA	420	103.0
OM*−P−OM*	780	120.0
CH2R5−CH1R6−CH0*, CH2R5−CH1R5−CH0*	540	104.5
CH1R5−CH0*−CH1R6	540	104.5
CH1R6−CH2R5−CH2R5, CH1R5−CH2R5−CH2R5	540	104.5
CH2R6−CH2R6−CH1R6, CH2R6−CH2R6−CH0*	530	111.0
CH1R5−CH0*−CH3*, CH1R5−CH1*−CHn*, n = 2,3	520	109.5
CH2R5−CH1R5−CH1*	520	109.5
CH2R6−CH0*−X, X = C*, CH3*, CH1R6	520	109.5
CH2R6−CH1R6−CH0*, CH2R6−CH0*−CH1R5	520	109.5
CH1R6−CH1R6−CH0*, CH1R6−CH1R6−CH2R5	520	109.5
CH1R6−CH0*−CH3*	520	109.5
CH2R6−CH1R6−CH2R6, CH2R6−CH1R6−CH1R6	520	109.5
CH1R6−CH2R6−C*, CH1R6−CH2R6−C*HR6	530	111.0
CH2R6−C*−C*HR6, C*−C*HR6−CH2R6	615	124.0
CH2R6−C*−CH0*	530	112.0
CH0*−CH1R5−CH1*	520	109.5
C*−CH0*−CH1R6	520	109.5
C*HR6−C*−CH0*	615	124.0
CH1R6−OA−H	450	109.5
CH2R6−CH1R6−OA	520	109.5

TABLE 6: The Force Field Parameters for the Improper Dihedral Angle (ξ) Terms in PC Lipids

ξ type	ξ in terms of atom names	force constant K_ξ (kJ mol^{-1} rad^{-2})	ideal ξ (degree)
tetrahedral center	C3−C1−O21−C2	334.84617	35.26439
planar group	C21−O21−C22−O22	167.42309	0.0
planar group	C11−O11−C12−O12	167.42309	0.0

of ethane, which consists only of two methyl groups. Then, with the methyl parameters fixed at the predetermined value, the properties of the methylene group were determined by comparison with the physical properties of saturated hydrocarbons containing both methyl and methylene groups.

A similar strategy was adopted for determining the torsion angles and van der Waals parameters of the atoms contained in the head groups. Initial determination was by comparison with the physical properties of the smallest relevant molecule, and with those properties fixed at the predetermined value, the properties of the additional groups added on could be determined relatively unambiguously.

2.1. General Methodology. Figure 1 shows the topology and labeling scheme for a united atom model for DPPC. Whenever possible, the force field parameters from the GROMOS96 43A1 parameter set[22] were adopted. In all molecular dynamics (MD) simulations and energy minimizations, GROMACS (version 3.1.4) modeling software[12] was used. When calculating molecular mechanics (MM) torsional profiles in the course of parametrization, GROMOS96 MD software[22] was used because of its capability of restraining dihedral angles. In all cases, standard GROMOS96 energy functions were used. For all MD simulations and MM calculations, all bonds were constrained with either the SHAKE[26] algorithm for GROMOS96 or the LINCS algorithm[8] for GROMACS. Twin-range cutoffs 1.0/1.6 nm were used for the van der Waals interactions. Particle mesh Ewald summation[50] with a real space cutoff of 1 nm was used for long-range electrostatic interactions. Nonbonding interactions involving the first and second neighbors were excluded in all MM/MD calculations. For quantum mechanical (QM) calculations, GAUSSIAN03[27] was used.

TABLE 7: Force Field Parameters for the Torsional Angles Using (a) Equation 1 and (b) Equation 2 in PC Lipids

(a)

torsion angle	force constant, K_ξ (kJ mol^{-1})	phase shift cos ξ	multiplicity m
C33−N−C32−C31	7.75	+1	3
C32−C31−O32−P	3.77	+1	3
C31−O32−P−O31	3.14	+1	3
C31−O32−P−O31	1.05	+1	2
O32−P−O31−C3	3.14	+1	3
O32−P−O31−C3	1.05	+1	2
P−O31−C3−C2	3.77	+1	3
O31−C3−C2−C1	5.92	+1	3
C3−C2−C1−O11	5.92	+1	3

(b)

	C_n (n = 0, 1,..., 5)	1−4 exclusion
N−C32−C31−O32	9.5761, 18.1619, −5.7260, −34.7386, 10.1726, 2.5538	no
C2−C1−O11−C11	1.6208, 7.7937, 5.3119, −12.0422, −3.6908, 3.5848	no
C3−C2−O21−C21	8.18, 2.04, 0.0, −8.72, 0.0, 0.0	no
Cn−On1−Cn1−Cn2, n = 1, 2	54.9582, −9.5297, −38.6803, −6.7482, 0.0 0.0	yes
On1−Cn1−Cn2−Cn3, n = 1, 2	3.9135, 0.9352, −3.6895, −4.1205, 2.0273, 0.9340	yes
Cn1−Cn2−Cn3−Cn4, n = 1, 2	3.6097, 19.6399, 14.0532, −41.7525, −9.8933, 15.2582	yes
Cm−Cm+1−Cm+2−Cm+3, m = 12, 22	6.4647, 16.7016, 4.8515, −28.0178 0.0 0.0	yes

TABLE 8: Densities and Heats of Vaporization ΔH_{vap} for Hydrocrbon Liquids at 298 K

hydrocarbon	density (g/cc)		ΔH_{vap} (kJ/mol)	
	experiment[e]	simulation	experiment[e]	simulation
ethane	0.5446[a]	0.5392[a]		
propane	0.493	0.4811	14.8	15.4
butane	0.573	0.5695	21.62	21.9
butane	0.6012[b]	0.5967[b]		
hexane	0.6548	0.6556	31.5	31.2
octane	0.6986	0.7002	41.5	39.8
decane	0.7266	0.7281	51.4	50.4
dodecane	0.7495[c]	0.7496[c]	61.5	60.3
pentadecane	0.7648	0.7626	76.8	76.3
heptadecane	0.7780[c]	0.7786[c]	86.5	84.8
isobutane	0.551	0.5511	19.1	18.1
isopentane		0.6166	24.5	23.1
isopentane	0.6201[c]	0.6215[c]		
isohexane	0.6532	0.6551	30.0	27.5
neopentane	0.5852	0.5874	22.4	20.8
cis-butene	0.616	0.6193	22.16	23.9
cis-2-pentene	0.6431	0.6504	26.86	28.4
cis-2-hexene	0.6869[c]	0.6841[c]	32.19	33.2
cis-5-decene	0.7445[c]	0.7414[c]		52.3
2-methyl-2-pentene	0.6863[c]	0.6859[c]	31.6	31.8
2,3-dimethyl-2-butene	0.7080[c]	0.7068[c]	32.51	30.9
cis-pentane	0.7457[c]	0.7441[c]	29.2	28.1
methylcyclopentane	0.7486[c]	0.7482[e]	31.64	31.4
cis-hexane	0.774	0.7741	33.7	32.3
methylcyclohexane	0.7694[c]	0.7682[c]	35.4	32.1
trans-decalin	0.8699	0.8664	46.2, 48.5	44.9
cis-hexene	0.811[c]	0.8103[c]	33.47	35.9
cholestane	0.909[d]	0.9114[d]		
cyclohexanol	0.9624[c]	0.9234	63.2	63.6
acetone	0.7845	0.8086	31.0	36.7
methyl acetate	0.9342[c]	0.9432[c]	32.3	40.2

[a] 184 K. [b] 273 K. [c] 293 K. [d] 361 K. [e] Reference 36.

Our van der Waals (VDW) parameters were determined using the general method perfected by several groups.[2,4] In this procedure, VDW parameters for the atom types in a connected subset of atoms within a lipid molecule are optimized to reproduce, in MD simulations, the experimental densities and heats of vaporization of "model" compounds that are identical or nearly identical to the target molecular group. For example, *n*-alkane chains serve as model compounds for saturated lipid hydrocarbon chains. The VDW interactions are calculated as a sum over all interacting nonbonded atom pairs i,j using a 12−6

Lennard−Jones (LJ) potential function with parameters $C6$ and $C12$,

$$V_{LJ}(r) = 4\varepsilon_{ij}[(\sigma/r_{ij})^{12} - (\sigma_{ij}/r_{ij})^{6}] = C12_{ij}/r_{ij}^{12} - C6_{ij}/r_{ij}^{6} \quad (1)$$

where ε_{ij} is the depth of the potential well, σ_{ij} is the distance at which the interparticle potential is zero, and r_{ij} is the distance between the particles. The parameters $C12_{ij}$ and $C6_{ij}$ are obtained, by geometric combination rules,[44] from $C12_{ii}$, $C12_{jj}$ and $C6_{ii}$, $C6_{jj}$

$$C12_{ij} = (C12_{ii}\, C12_{jj})^{1/2} \qquad C6_{ij} = (C6_{ii}\, C6_{jj})^{1/2} \quad (2)$$

The most important new results described here, improved torsional parameters for phospholipid head group dihedrals, were determined using the procedure outlined by Reiling et al.[17] In this method, a potential energy profile as a function of the dihedral angle is computed at the ab initio level. Then torsional parameters are fitted to this profile in an analytical molecular mechanical potential energy function, utilizing the new VDW parameters as described above. In this work, we used GAUSSIAN03[27] for ab initio calculations at the B3LYP/6-31G(d,p) level with all other geometrical parameters optimized. In cases where the resultant potential function could be well fit with a single cosine function, the analytical function was

$$V_{dih}(\phi) = K_{\phi}(1 + \cos(\delta)\cos(m\phi)) \quad (3)$$

where K_{ϕ} is the force constant for the particular dihedral function, δ is either 0 (for rotation around a single bond) or π (for rotation about a double bond), and m is an integer. Note that we use the convention that the cis conformation corresponds to $\phi = 0$.

In some cases, the form of eq 3 was not adequate, so that we used a function of the form

$$V_{dih}(\phi) = \sum_{n=0}^{m} C_n \cos(n(\phi - \pi)) \quad (4)$$

In the actual fitting, we used either $m = 3$, corresponding to the form of the Kuwajima potential,[9] or $m = 5$, corresponding to the form of the Ryckaert−Bellemans potential.[18] The shift of π radians in the torsion angle on the right-hand side of eq 4 is to account for the fact that in refs 9 and 18, a different convention is used for the phase of the torsion angle, so that in the details of those papers, the dihedral angle is shifted 180° from the convention in Gromacs.

2.2. Parameterization for Lipid Hydrocarbon Chains. The force field parameters for the bond stretching and bond angle terms for the hydrocarbon chains were all taken from the GROMOS96 43A1 parameter set and were accepted throughout this work. For united atom (UA) hydrocarbons, each atom was assigned to a zero charge. Improper dihedral parameters from the GROMOS96 43A1 parameter set were used for planar groups (out of plane) and tetrahedral centers (out of tetrahedral configuration).

2.2.1. Normal (Not 1−4) van der Waals Parameters. The normal VDW parameters for CH2* and CH3* were determined by the following iterative process. The normal VDW parameters for CH3* were determined by MD simulation of liquid ethane at low temperature to reproduce the experimental density and heat of vaporization ΔH_{vap} of liquid ethane, CH_3-CH_3. To obtain the VDW parameters for CH2*, MD simulations for liquid pentadecane were carried out by using the initially optimized VDW_{CH3*} parameters and then adjusting the values of the VDW_{CH2*} parameters to reproduce the observed density and ΔH_{vap} for liquid n-pentadecane. The rationale for choosing n-pentadecane at this point in the iteration is that the results for a long-chain hydrocarbon are strongly dependent on the CH2* parameters since the ratio of CH2*/CH3* is so high in this molecule. The next stage in the iteration involves returning to short-chain hydrocarbons by utilizing the pentadecane-derived VDW_{CH2*} parameters in MD simulations for liquids n-butane and n-hexane, adjusting their VDW_{CH3*} to reproduce their experimental densities and ΔH_{vap}. A final refinement of the VDW_{CH2*} parameters was achieved by using the new VDW_{CH3*} parameters in MD simulations for liquid n-pentadecane to reproduce its experimental density and ΔH_{vap}. The resultant VDW parameters accurately reproduce the saturated straight-chain liquid hydrocarbon density and ΔH_{vap} over a wide range of chain lengths (see Figure 2). We note that during this step, we found that we needed a van der Waals cutoff of at least approximately 1.5 nm to create hydrocarbon force fields that would be transferable across hydrocarbon chains of multiple lengths. Specifically, a cutoff of 1.2 nm would not work adequately. All parameters in the 43A1-S3 force field were created using a VDW cutoff of 1.6 nm, and we recommend this cutoff for application of the force field.

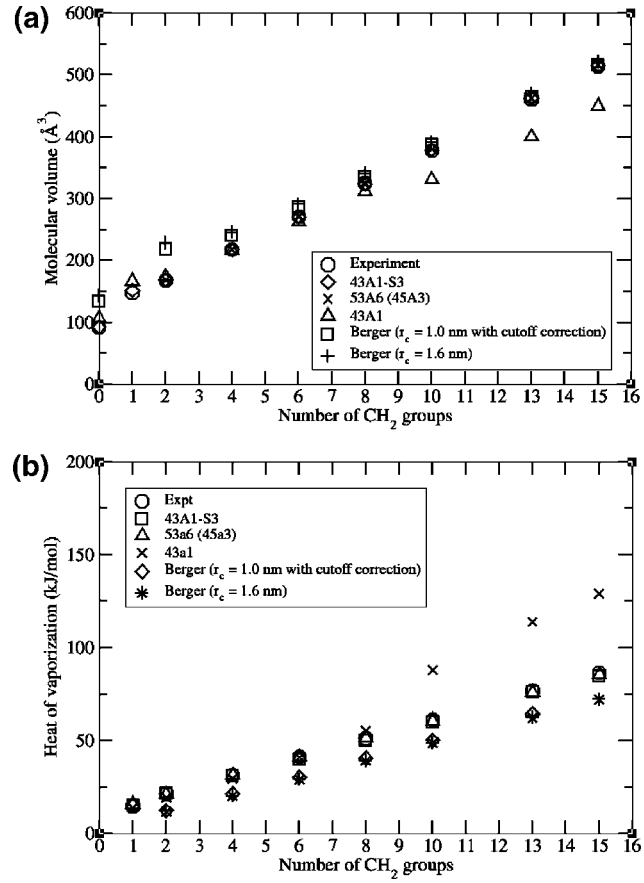

Figure 2. (a) Molecular volumes of n-alkanes as a function of the number of methylene groups CH_2. (b) Standard heats of vaporization ΔH_{vap} of n-alkanes at 298 K as a function of the number of methylene groups CH_2.

Other robust united atom (UA) *n*-alkane force fields exist, such as the OPLS-UA (optimized potentials for liquid simulations) of Jorgensen et al.,[37] TraPPE (transferable potentials for phase equilibria) of Martin and Siepmann,[38] NERD (Nath, Escobedo, and de Pablo revised force field) of Nath et al.,[39] and GROMOS 53A5/53A6 of Oostenbrink et al.[40] Note that the 53A5/53A6 alkane force field parameters come from the GROMOS 45A3 parameter set.[41] A comparison of the *n*-alkane LJ parameters of these force fields as well as the one (43A1-S3) developed in this work is shown in Table 1. Despite different parametrization strategies, both TraPPE and 43A1-S3 force fields have the same σ and ε/k_B values for CH3 (methyl atom) and very similar σ and ε/k_B values for CH2 (methylene atom). The former is based on calculations of vapor−liquid coexistence curves of *n*-alkanes, and the latter, as presented in this paper, is based on computations of liquid alkane densities and ΔH_{vap}. The fact that these independent approaches converge to essentially the same parameters means that both parameter sets can describe both the vapor−liquid coexistence curves and also the specific volumes and heats of vaporization.

2.2.2. n-Alkane Torsional Parameters. In the course of determining the VDW parameters for the atom types CH2* and CH3* in *n*-alkanes, the form of the Kuwajima potential, $V_{KW}(\phi)$,[9] was used for the dihedral terms involving these atom types. The Kuwajima potential has the same functional form as eq 4, with $m = 3$. The $C_n$values were parametrized by fitting to the torsional profile calculated at the CCSD(T)/6-31G(2df,p)// B3LYP/6-31G(2df,p) level for the central dihedral of *n*-hexane with both terminal CH3 groups trans to their corresponding third-neighbor CH2 groups. The $V_{KW}(\phi)$ form for the dihedral terms for *n*-alkanes includes 1−4 nonbonded interactions; therefore, when this form is used, the 1−4 pairs are excluded from the nonbonded pair list. Previous Gromos 43A1 force field parameters for bond lengths and bond angels of *n*-alkanes were used. We assume that the values thus derived for the central dihedral of *n*-hexane (CH2*−CH2*−CH2*−CH2*) are applicable to all dihedral types CH*n**−CH2*−CH2*−CH*n** (*n* = 2, 3) of *n*-alkanes. We have explicitly explored the validity of this assumption by computing $V_{KW}(\phi)$ with the method above for *n*-butane. We found no significant difference in the relative energy levels of the three minima and only about a 1−2 kJ/mol difference in transition barriers, as compared to the central dihedral for *n*-hexane (Figure 3a).

2.2.3. Cases Where 1−4 Nonbonded Interactions Must Be Considered Explicitly. The Kuwajima torsion parameters for saturated bonds in *n*-alkanes, as described above, implicitly include the nonbonded 1−4 interactions. In the case of saturated hydrocarbon ring structures, for example, cyclohexane, applying the Kuwajima potential as derived above will cause double counting of the 1−4 interactions. To deal with this problem, a separate torsion function for alkanes, KW_{14}, was constructed that does not include 1−4 nonbonded interactions. The use of KW_{14} implies the inclusion of specific 1−4 nonbonded interactions. The construction of KW_{14} and associated nonbonded interactions is described below. As in other constructions in this work, the process here is an iterative one.

To obtain 1−4 interactions when the 1−4 pair is CH3*−CH3*, *n*-butane is taken as the initial model system because in *n*-butane, the only intramolecular nonbonded interaction is the VDW_{14} interaction between the two methyl groups (CH3*). To obtain the VDW_{14} parameters for CH3*, a standard GROMOS96 torsional function $V_{dih}(f)$ for alkyl chains was selected. We adopted the torsional parameters ($K_f = 5.92$ kJ /mol, $\delta = 0.0$, and $m = 3$) from the GROMOS96 45A3 parameter set.[23] The

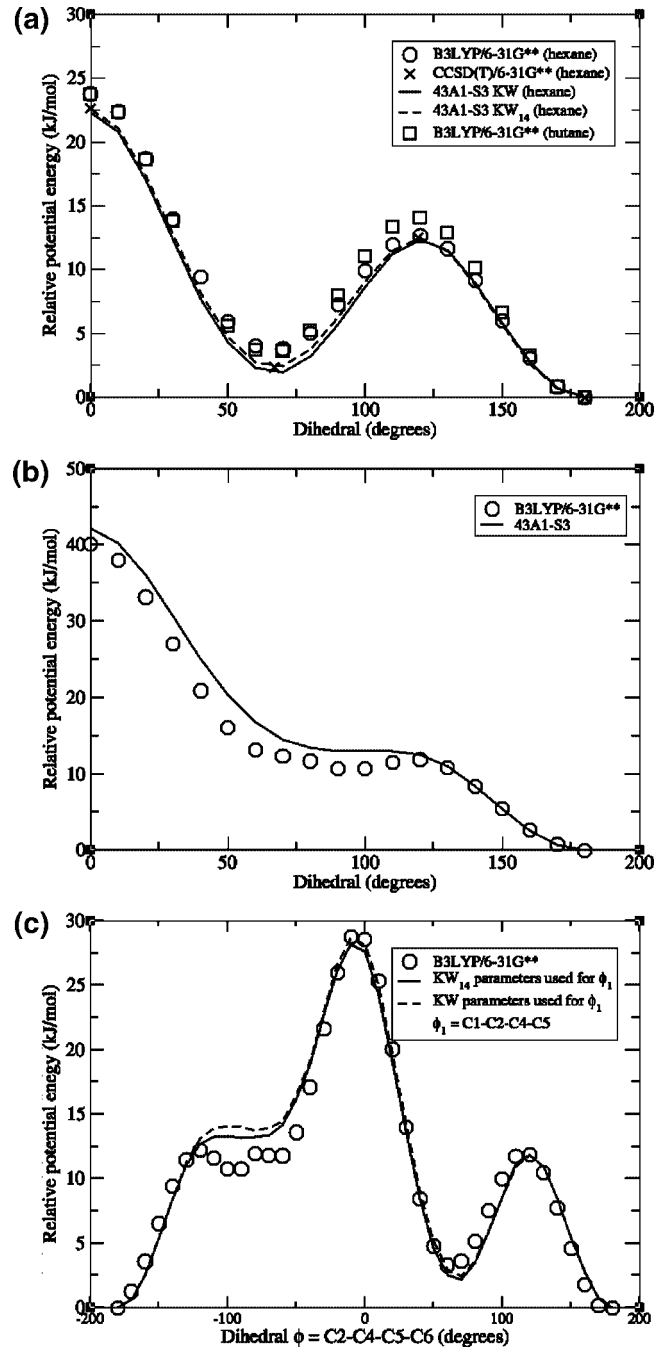

Figure 3. (a) Torsional energy profiles for *n*-butane and the central dihedal of *n*-hexane. (b) Torsional engy profile for the dihedral C−CH_2−CH_2−CH_3 (CH0*CH2*CH2*CH3*) of 2,2-dimethylpentane ($(CH_3)_3CCH_2CH_2CH_3$). (c) Torsional energy profiles for the dihedral ϕ (C2−C4−C5−C6) of isohexane

VDW_{14} parameters for CH3* were adjusted so that the function $V_{dih}(\phi)$ was best fit to the ab initio $V_{dih}(\phi)$ calculated at the CCSD(T)/6-31G(2df,p)//B3LYP/6-31G(2df,p) level. These VDW_{14} parameters for CH3* were then adopted for terminal methyls in *n*-pentane, and *n*-pentane was used as a model system. An analogous procedure to that used for *n*-butane was applied to obtain the VDW_{14} parameters for CH2*. In calculating the $V_{dih}(\phi)$ profiles for *n*-pentane, rotation around one of the two dihedrals centered on a CH2*−CH2* bond was set as the reaction coordinate, while the other was kept in a trans configuration (but permitted to be optimized within that configuration). The 1−4 VDW parameters for CH2*−CH3* were taken as the geometric mean of the CH2*−CH2* and

CH3*−CH3* parameters. The VDW_{14} parameters for CH2* and CH3* optimized in this way are designed to be used for the methylene and methyl groups in other hydrocarbons

2.2.4. Branched Alkanes. For branched alkanes, there are two additional atom types, CH0* (the tetrahedral or SP3 bare carbon) and CH1* (the SP3 methine group) to be considered. The derivation of their parameters will be given below. For atom types CH2* and CH3* in branched alkanes, all bonding and nonbonding parameters were taken from those for *n*-alkanes. When branches occur at the atoms with sequence number j and k of a bond, there exists more than one dihedral angle ijkl. In the case where the atoms j and k are CH2*, the above-described KW_{14} dihedral is used, and explicit 1−4 interactions between all of the atoms in the 1−4 position are added, except for a special case that will be described below.

*CH0**. The VDW parameters for CH0*, the central tetrahedral carbon of neopentane, $C(CH_3)_3$, were parametrized to reproduce the observed density and ΔH_{vap} for liquid neopentane. To obtain the VDW_{14} parameters for CH0* and torsional parameters involving CH0*, we used 2,2-dimethylpentane ($(CH_3)_3CCH_2CH_2CH_3$) as the model molecule. Initially, the VDW_{14} parameters for CH0* were set to those for the bare carbon (CH0) from the GROMOS96 43A1 parameter set. The parametric values of KW for *n*-alkanes were taken for the dihedral CH3*−CH0*−CH2*−CH2*. We found that the GROMOS96 torsional parameters for alkanes plus the VDW_{14} for the bare carbon CH0 gave a very good fit to our ab initio calculations for the dihedral angle ϕ involving CH0*CH2* CH2*CH3* (Figure 3b). Hence, the VDW14 parameters for the tetrahedral carbon (CH0) from the 43A1 parameter set were taken for CH0* in this work without further refinement.

*CH1**. The normal VDW parameters for CH1* were determined from MD simulations for liquids isobutane $(CH_3)_2CHCH_3$ and isopentane $(CH_3)_2CHCH_2CH_3$ by reproducing their corresponding experimental density and ΔH_{vap} values. For determination of the VDW_{14} parameters for CH1* and the torsional parameters for the dihedral type involving CH1*, isohexane $(CH3)_2CHCH_2CH_2CH_3$ was used as a model molecule (Figure 4). The GROMOS96 dihedral function (eq 2 with $K_f = 5.92$ kJ/mol, $d = 0$, and $m = 3$) for alkanes was initially applied to the dihedral angle ϕ = C2−C4−C5−C6 (CH1*−CH2*−CH2*−CH3*), and the KW_{14} torsional parameters were applied to one of the dihedral angles f_1 = C1−C2−C4−C5 (CH3*−CH1*−CH2*−CH3*). The tetrahedral center (CH1*) was set according to the GROMOS96 improper dihedral parameter set with type code gi-2. Other parametric values as set in the current 43A1-S3 force field set and are not reprinted here. The VDW_{14} parameters for CH1* were then parametrized so that the function $V(\phi)$ was fitted to the ab initio $V(\phi)$, where ϕ = C2−C4−C5−C6 (Figure 4). The two geminal methyl groups (C1 and C3) were trans and gauche to C5 in the course of calculations of $V(\phi)$. Figure 3c shows the fitted $V(\phi)$ profiles as compared to the $V(\phi)$ calculated at the B3LYP/6-31G(d,p) level. From the same figure, one may observe that use of the KW torsional parameter set for ϕ_1 = C1−C2−C4−C5 (CH3*−CH1*−CH2*−CH3*) also gives the same extent of good agreement of the fitted $V(\phi)$ with the ab initio $V(\phi)$. As can be seen from Figure 3c, the use of the GROMOS96 dihedral function for ϕ (eq 3 with $K_f = 5.92$ kJ/mol, $d = 0$, and $m = 3$) is adequate in the range of ϕ from $-\pi$ to π. Hence, this potential was assigned to use for dihedral angles involving CH1* without further parametrization.

2.2.5. n-Alkenes. The same parameter sets (VDW, VDW_{14}, bond stretching, bond angle, dihedral angle) derived for *n*-alkanes were used in *n*-alkenes for the corresponding atom, bond, bond angle, and dihedral angle types not involving the unsaturated methine group (atom type C*H1). In the course of parametrization for the force field terms involving C*H1, the GROMOS 96 bond strectching and bond angle parameters were accepted. The double bond dihedral angle parameters (eq 3 with $K_f = 101.3$ kJ/mol, $\delta = \pi$, and $m = 2$) were taken from Smith and Paul.[28] The parametrization procedure for alkenes is in a progressive manner as that for alkanes. *cis*-Alkenes (2-butene,

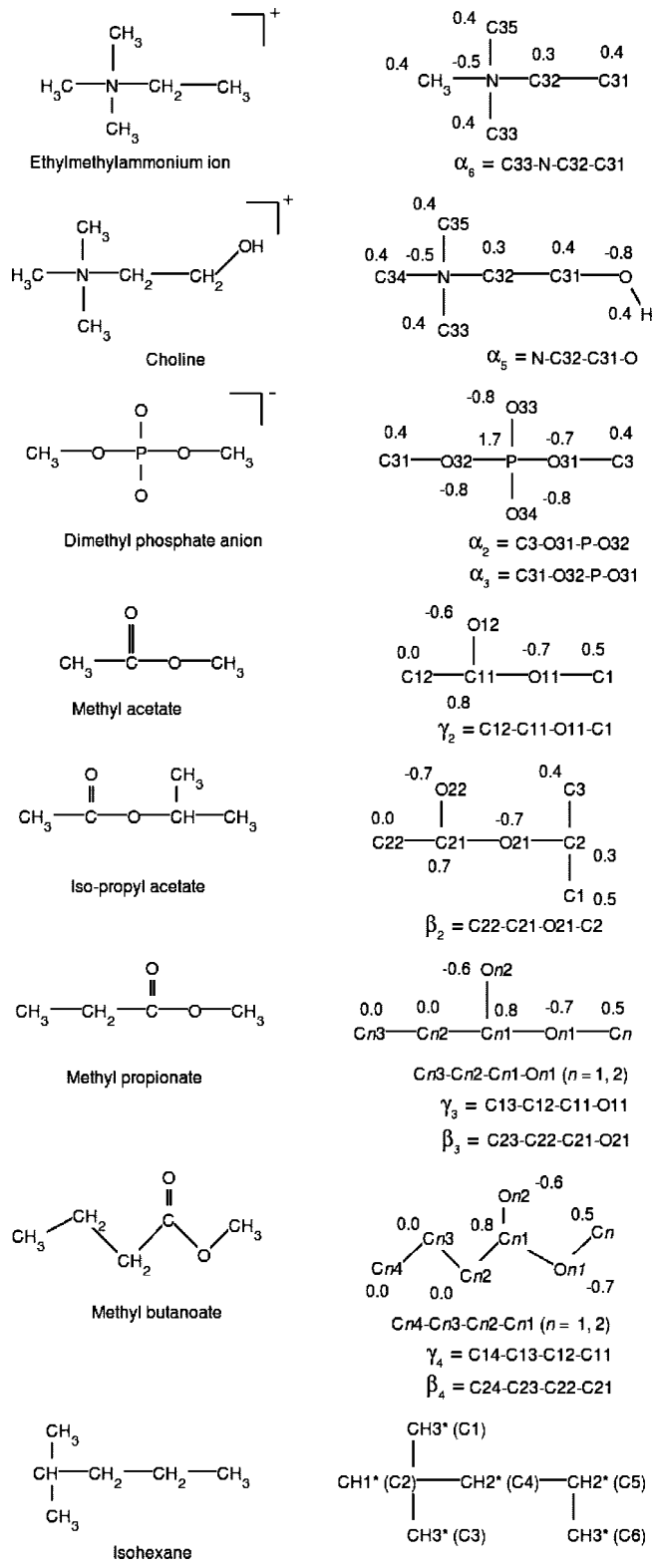

Figure 4. Molecular species used to model to the fragments of the lipid polar region.

TABLE 9: Simulated Densities and Heats of Vaporization ΔH_{vap} for Acetone and Methyl Acetate at 298 K

	density (g/cc)			ΔH_{vap} (kJ/mol)		
	43A1-S3	53A5[a]	expt.[b]	43A1-S3	53A5[b]	expt.[b]
acetone	0.809	0.653	0.784	36.7	31.3	31.3
methyl acetate	0.938	0.977	0.928	40.2	33.2	32.3

[a] Reference 40. [b] Experimental values taken from ref 40.

2-pentene, 2-hexene, and 5-decene) were employed as model molecules for parametrization.

2.3. Parameterization for Lipids: Polar Groups. ***2.3.1. van der Waals Parameters.*** Having optimized hydrocarbon chain interaction parameters such as those from GROMOS96 45A3[41] alone does not guarantee that the MD simulation gives an area per lipid in agreement with experimental values.[4,29] Although the variants of the 45A3 parameter sets combined with our charge set for lipid yield simulated an area per DPPC in agreement with experiment, the burden is put on increasing the repulsive $C12$ parameter of the planar ester carbon alone.[29] Re-evaluation of the VDW parameters for the polar atoms of the PC head group is hence necessary.

Our approach of parametrization is to use small organic molecules which may closely represent the polar fragments of the PC head group. For example, methyl acetate (CH_3COOCH_3) is used to mimic the ester fragments (Figure 4). The LJ parameters derived from calculations of the density and ΔH_{vap} for liquid methyl acetate are assumed to be transferrable to the ester fragments for membrane simulations. In order to be consistent, the partial charges on the model molecules are set to those on the fragments and are not optimized in the course of parametrization. Since electrostatic interactions play a more important role than VDW interactions in the determination of intermolecular interactions for polar liquids, optimizing VDW parameters alone would not give good fits of density and ΔH_{vap} to experimental data simultaneously. Since our primary concern is to have a lipid force field that can predict membrane structures (such as area per lipid, membrane thickness, etc.) comparable to experimental values, we choose to select VDW parameters that will give reliable volumetric properties.

Ester Fragment. For the ester fragment, we have three atom types (carbonyl carbon, carbonyl, and ester oxygen) whose VDW parameters needed to be reexamined and one target molecule (methyl acetate). Initially, acetone $(CH_3)_2CO$ was used to estimate the VDW parameters for the carbonyl group, C, and O. Gromos96 43A1 bonding parameters were used for the UA acetone. There is no intramolecular 1−4 interaction in this molecule, and hence, VDW_{14} parameters are not needed for MD simulation. The VDW parameters of atom type CH3* from this work were used for the methyl groups in acetone. The partial charges on the two CH3* atoms were set to zero (caculated Mulliken charges[46] on C, O, and each methyl group are 0.422, −0.428, and 0.003, respectively at the B3LYP/6-31G** level). The charges on C and O were set to +0.7 and −0.7 e, respectively, the same as those on the carbonyl group of the Sn-2 chain. VDW parameters of the SP2 bare carbon, C* (Table 3B), parametrized from alkenes were initially applied to the carbonyl C. The VDW parameters for the carbonyl O were then adjusted to give best fits of the density and ΔH_{vap} of acetone to the experimental values by MD simulations. Refinement of the VDW parameters for the carbonyl C was then carried out by using the newly obtained VDW parameters for O via MD simulations for liquid acetone. These final VDW parameters for C and O, which are now designated as CO* and O*, respectively, were then accepted in MD simulations of liquid methyl acetate CH_3COOCH_3. Gromos 43A1 bonding parameters were used for the model molecule. The partial charges on the UA model methyl acetate were set to those on the ester fragment of the Sn-1 chain (Figure 4). They were not changed in the course of parametrization. By using eq 4, the KW torsional parameters (which implicitly include all 1−4 interactions) for the dihedral $CH_3-C-O-CH_3$ were obtained by fitting to the quantum mechanically calculated potential energy profile (see also section 2.3.2.3). The only remaining VDW parameters to be optimized were those for the ester oxygen (atom type OA). Our initial guess was to use the 43A1 parameters for OA. Despite our numerous trials, we could not find any set of VDW parameters for OA that gave the caluculated density and ΔH_{vap} simultaneously in good agreement with the experimental data. We found that the original 43A1 VDW parameters for atom type OA combined with those of CO* and O* gave satisfactory results on the computed density and ΔH_{vap} for liquid methyl acetone. The calculated results using 53A5[40] and 43A1-S3 force fields are listed in Table 9. While the 53A5 force field gives ΔH_{vap} values for acetone and methyl acetate in good agreement with experiments, its absolute mean deviation of their densities (11%) from experiments is larger than that (2%) of the 43A1-S3 results (Table 9).

Choline and Phosphate Fragments. The nonexistence of pure liquid states of choline and phosphate does not permit us to parametrize the VDW parameters of the atoms involved in these fragments. We therefore accept the 43A1 VDW/VDW_{14} paramteters for phosphate P (atom type P), choline N (atom type NL), and phosphate ester oxygen O31/O32 (atom type OA) in this work, except the phosphate oxygen O33/O34 (atom type OM).

In GROMOS parameter sets, the choice of the parameters $C12_{ii}$ and $C6_{ii}$ to be used in eq 2 depends on the types of atoms involved and their character of interaction. Up to three different $C12$ parameters [$C12(1)$, $C12(2)$, and $C12(3)$] are defined for each atom type (Table 3A, columns 3, 4, and 5). The choice of the $C12$ parameter to be used for atom type I and atom type J in eq 2 is predefined in a matrix.[22,40] In the 43A1 parameter set, the $C_6^{1/2}$ parameters for atom types O and OM are the same. In addition, the $C_{12}^{1/2}$ (O,O), $C_{12}^{1/2}$ (OM,OM), and $C_{12}^{1/2}$ (O,OM) parameters have the same value. That is, the same $C12(1)$ value is used for atom type O and atom type OM. Following the GROMOS 43A1 rules, we assign the $C_6^{1/2}$ (O*,O*) value to the phosphate oxygen, which is now designated as atom type OM*, and the set $C12(1)$ value of atom type OM* to that of atom type O*.

2.3.2. Torsional Parameters. The molecular fragments used to parametrize the PC polar group are shown in Figure 4. For the most part, torsional parameters for the dihedral angles involving the polar head group atoms were reparameterized by reproducing the corresponding ab initio torsional profiles. All VDW parameters needed were taken from Table 3A and B.

The charges for the PC lipid, as listed Table 2, were accepted in the course of parametrization for the torsional parameters involving the head group atoms. As in the cases for hydrocarbons, the parametrization procedure was progressive, and when

the standard one-term trigonometric function for a dihedral angle in interest did not yield satisfactory results, a torsional function like the Ryckaert−Bellemans (RB)[18] or Kuwajima (KW)[9] potential was used instead. The PC head group consists of choline and phosphate fragments as well as two ester groups which link the head group and the hydrocarbon tails (Figure 1). Figure 4 illustrates the model systems used for modeling the dihedrals for these fragments. Partial charges assigned to the atoms of these fragments and the dihedrals of interest are also displayed in the figure. The most important changes in the 43A1-S3 are the PC polar group torsion parameters, which are described below.

2.3.2.1. The Choline Group. Torsional parameters for the dihedral C34−N−C32−C31 (α_6) were fitted to the corresponding ab initio torsional profile for ethyltrimethylammonium $[(CH_3)_3\ NCH_2CH_3]^+$. They were in turn used for modeling the torsional parameters for the dihedral N−C32−C31−O32 (α_5) of the choline fragment (Figure 4)

2.3.2.2. The Phosphate Group. The dihedrals of the phosphodiester group, C31−O32−P−O31 (α_3)/C3−O31−P−O32 (α_2), were modeled by using dimethyl phosphate (DMP) as the model system. The potential energy surface (PES) of DMP as a function of the two P−O single bonds is a complex one, with local minima at the gauche−gauche, trans−gauche, and trans−trans conformations.[30−33] To simplify the situation, we kept one P−O torsion (α_3) in the trans conformation initially and calculated the PES as a function of α_2. Using the torsional parmeters X-P-OA-X from the GROMOS96 43A1 parameter set, we found that the molecular mechanics (MM) torsional profile matched the ab initio torsional profile (Figure 5a).

2.3.2.3 The Ester Group Region. Linking the head group and the hydrocarbon tails of PC lipids are two ester groups (Figure 1). Methyl acetate CH_3COOCH_3 (Figure 4) was used to model the methyl acetate fragments C12−C11(O12)−O11−C1/C22−C21(O22)−O21−C2 in optimizing the torsional parameters for the dihedrals C12−C11−O11−C1 (γ_2) and C22−C21−O21−C2 (β_2). These optimized torsional parameters were then accepted in parametrizing the torsional parameters of the dihedrals C13−C12−C11−O11(γ_3) and C23−C22−C21−O21 (b_3) using methyl proprionate as a model system. The dihedrals b_2 and g_2 were placed in the trans conformation initially in calculating the torsional profiles for b_3 and g_3, respectively. By accepting the optimized parameters for γ_2 and γ_3, the torsional parameters for the dihedrals C14−C13−C12−C11 (γ_4) and C24−C23−C22−C21 (β_4) of the methylbutanoate fragment were parametrized to reproduce the corresponding ab initio torsional profiles. Finally, the torsional parameters for the dihedrals C2−C1−O11−C11 (γ_1) of the ethyl acetate fragment (modeled with ethyl acetate $CH_3COOCH_2CH_3$) and C3−C2−O21−C21 (β_1) of the isopropyl acetate fragment (modeled with isopropyl acetate $CH_3COOCH(CH_3)_2$) were optimized to fit the corresponding quantum mechanically calculated energy profiles. It should be noted that the general torsional parameters for X-CHn-OA-X from the GROMOS96 43A1 parameter set were accepted for the dihedral P−O32−C31−C32 (α_4)/P−O31−C3−C2 (α_1). As can be seen from Figure 5, the MM calculated torsional energy profiles with the 43A1-S3 parameters for the dihedrals α's, β's, and γ's agree well with the ab initio results.

2.4. Parameterization for Cholesterol Using Cyclic Hydrocarbons. Cholesterol is a complicated molecule with fused five- (*c*-pentane) and six-membered (*c*-hexane and *c*-hexene) rings. We find that the united atom model cholesterol requires special ring carbon types, which are not presently in Gromacs. Therefore, we have created the new united atoms CH1R5, CH2R5, CH2R6, and C*HR6 for 43A1-S3, where the number at the end of the united atom name denotes the number of carbons in the ring. (Note that we do not include a * in the names of some of these united atoms, despite the fact that they are newly derived for 43A1-S3. This is because atom names in Gromacs are limited to five characters in its output coordinate files.) To characterize the force field parameters for cholesterol, simple cyclic hydrocarbons such as *c*-pentane, *c*-hexane, *c*-hexene, methyl-*c*-hexane, *t*-decalin, and cyclohexanol were used as model molecules for parametrization, as discussed below.

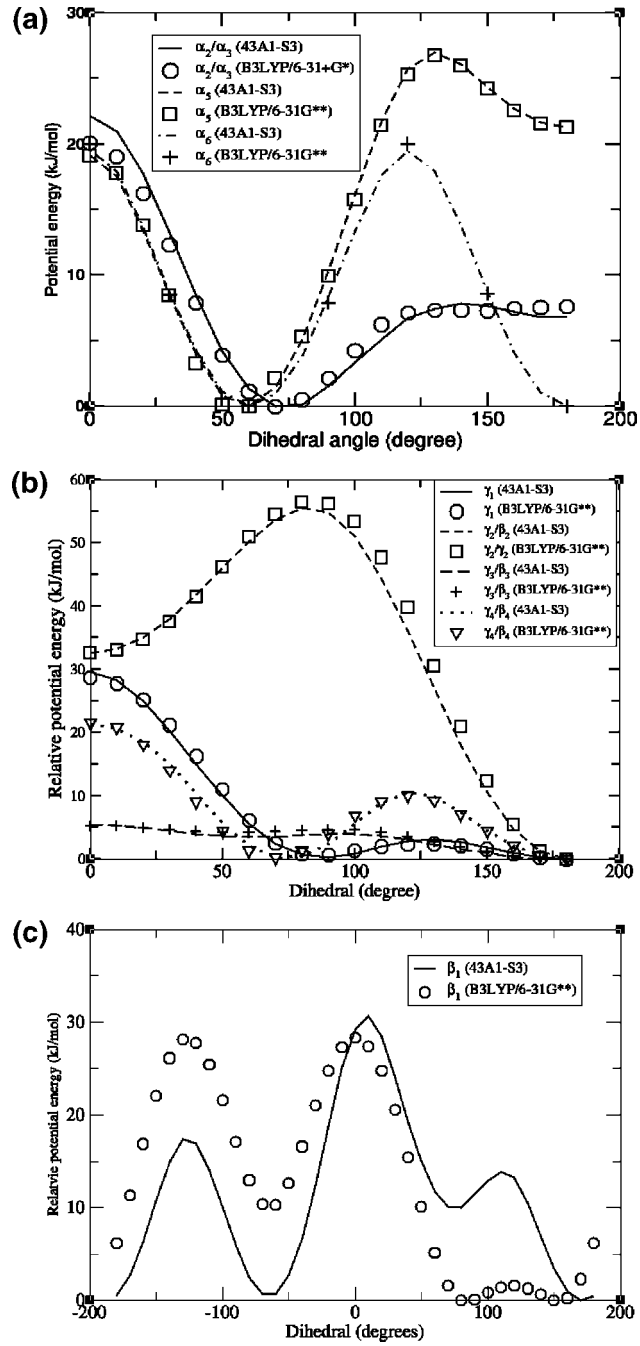

Figure 5. Relative potential energy profiles for the dihedrals of the head group. (a) α's of the choline and phosphate groups. (b) γ's and β's of the ester regions. (c) β_1 of the ester group of the Sn-2 chain. Refer to Figure 1 for the definitions of α, β, and γ dihedrals.

2.4.1. c-Pentane and Methyl-c-pentane. For five-membered rings, the nonbonding 1−4 interactions involving the ring atoms can also be considered as the corresponding nonbonding 1−3

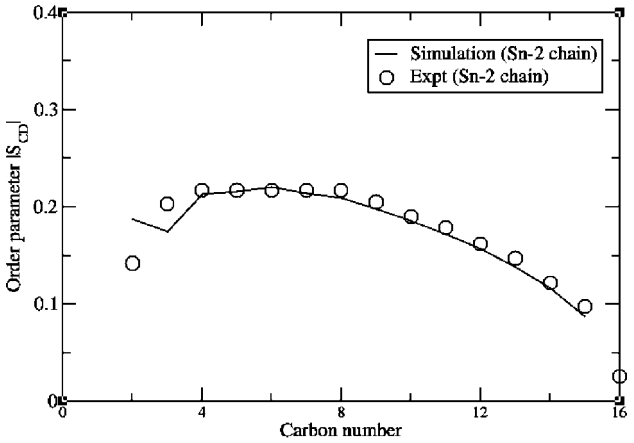

Figure 6. Calculated and observed order parameters for the Sn-2 chain of DPPC.

interactions. Hence, all nonbonding interactions between ring atoms are ignored since nonbonding interactions involving the first and second neighbors are excluded as a general rule. These ring compounds invovle two new atom types, CH2R5 (the CH2 groups of *c*-pentane and methyl-*c*-pentane) and CH1R5 (the CH group of methyl-*c*-pentane). Their VDW_{14} parameters were set to those of CH2* and CH1*, respectively. Bond stretching and bond angle force constants were taken from those for alkanes in the 43A1 pamameter set. The corresponding ideal bond lengths and bond angles were set to those of the B3LYP/6-31G(d,p) optimized structures. The normal VDW parameters for the CH2 groups (atom type CH2R5) in *c*-pentane were parametrized via MD simulation to reproduce its density and ΔH_{vap}. The so-obtained VDW parameters for CH2R5 were in turn applied to methyl-*c*-pentane in order to parametrize the VDW parameters for CH1R5.

2.4.2. c-Hexane and Methyl-c-hexane. The atom types CH2R6 and CH1R6 represent the CH2 and CH groups, respectively, of the six-membered rings. The bond stretching and bond angle parameters involving these atoms types were set to those for *n*-alkanes. The torsional parameter set KW_{14} was accepted for dihedral types CH*n*R6−CH*n*R6−CH*n*R6−CH*n*R6 ($n = 1, 2$). The VDW_{14} parameters for CH1R6 and CH2R6, the same as those for CH1* and CH2*, respectively, are listed in Table 3B. Optimization for the normal 6−12 VDW parameters for CH*n*R6 followed the same way as that for CH*n*R5. Their parametrized values are listed in Table 3B.

2.4.3. t-Decalin (Bicyclo[4.4.0]octane). This fused ring molecule has two atom types CH1R6 and CH2R6. Thus, all of the force field parameters for this model molecule are the same as those used in *c*-hexanes. We find that neglecting 1−4 nonbonded interactions involving atoms from different rings yields essentially the same density and ΔH_{vap} values as including them (both in good agreement with experimental data) and that the energy-minimized geometry is also in agreement with the B3LYP/6-31G(d,p) optimized structure. For this reason, we neglected 1−4 interactions between atoms in different fused rings in all molecules in which those atoms were not charged, such as cholestane and cholesterol, in addition to *t*-decalin.

2.4.4. c-Hexene. The atom types of the unsaturated methine and methylene groups are CHR6 and CH2R6, respectively. The bonded force field parameters for *n*-alkenes were accepted for *c*-hexene, except that the ideal bond angle for CH═$CHCH_2$ (CHR6−CHR6−CH2R6) was set to the value of the B3LYP/6-31G(d,p) optimized structure, 124°. For the

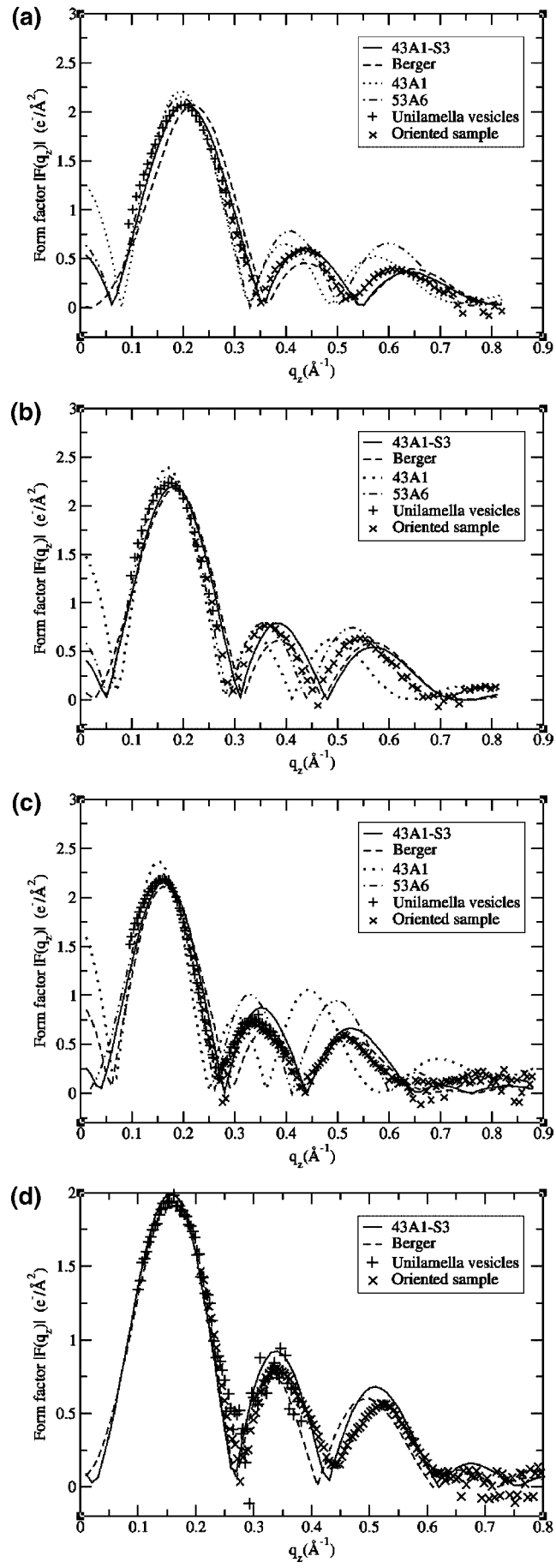

Figure 7. Simulated and observed form factors for fluid-phase lipid bilayers. (a) DLPC. (b) DMPC. (c) DPPC. (d) DOPC.

TABLE 10: DLPC Bilayer Structural Parameters from MD Simulations and Their Experimentally Derived Values

	DLPC at 303K			
	experiment[a]	43A1-S3	Berger[b]	53a6[c]
V_L (Å^3)	991	977	1013	968
D_B (Å)	31.4	31.0	31.0	34.3
D_{HH} (Å)	30.8	28.5[d] (30.0)[e]	27.8[d] (30.1)[e]	31.0[d] (32.8)[e]
$2D_C$ (Å)	20.9	20.7	20.7	23.3
A (Å^2)	63.2	63.0	65.4	56.4
A_G (Å^2)[f]		62.9	65.0	56.1

[a] Values taken from Table 2 of ref 42. [b] Values calculated in this work. MD simulations were carried out using the Lennard-Jones (LJ) parameters for lipid of Berger et al.[2] and the lipid charge set of Chiu et al.[3] [c] Values calculated in this work. MD simulations were carried out using the GROMOS 53a6 LJ and bonding parameters for PC lipid[40] and the lipid charge set of Chiu et al.[3] [d] Distance between the peaks in the total electron density profile. [e] Distance between the peaks in the atom density profile of phosphate groups. [f] *xy*-Plane area of the simulation box by the number of lipids per leaflet.

TABLE 11: DMPC Bilayer Structural Parameters from MD Simulations and Their Experimentally Derived Values

	DMPC at 303K			
	experiment[a]	43A1-S3	Berger[b]	53a6[c]
V_L (Å^3)	1101	1086	1112	1070
D_B (Å)	36.3	35.0	35.5	39.3
D_{HH} (Å)	35.3	32.6[d] (34.3)[e]	32.2[d] (34.4)[e]	34.9[d] (36.7)[e]
$2D_C$ (Å)	25.4	24.6	24.7	28.0
A (Å^2)	60.6	62.1	62.6	54.5
A_G (Å^2) [f]		61.8	62.6	54.3

[a] Values taken from Table 2 of ref 42. [b] Values calculated in this work. MD simulations were carried out using the Lennard-Jones (LJ) parameters for lipid of Berger et al.[2] and the lipid charge set of Chiu et al.[3] [c] Values calculated in this work. MD simulations were carried out using the GROMOS 53a6 LJ and bonding parameters for PC lipid[40] and the lipid charge set of Chiu et al.[3] [d] Distance between the peaks in the total electron density profile. [e] Distance between the peaks in the atom density profile of phosphate groups. [f] *xy*-Plane area of the simulation box by the number of lipids per leaflet.

TABLE 12: DPPC Bilayer Structural Parameters from MD Simulations and Their Experimentally Derived Values

	DPPC at 323K			
	experiment[a]	43A1-S3	Berger[b]	53a6[c]
V_L (Å^3)	1229	1209	1226	1193
D_B (Å)	39.0	38.0	37.3	42.4
D_{HH} (Å)	38.0	35.7[d] (37.2)[e]	34.7[d] (37.0)[e]	37.6[d] (40.2)[e]
$2D_C$ (Å)	28.4	27.6	27.7	31.4
A (Å^2)	63.1	63.6	65.7	56.3
A_G (Å^2)[f]		63.7	65.5	56.2

[a] Values taken from Table 3 of ref 43, third column. [b] Values calculated in this work. MD simulations were carried out using the Lennard-Jones parameters for lipid of Berger et al.[2] and the lipid charge set of Chiu et al.[3] [c] Values calculated in this work. MD simulations were carried out using the GROMOS 53a6 LJ and bonding parameters for PC lipid[40] and the lipid charge set of Chiu et al.[3] [d] Distance between the peaks in the total electron density profile. [e] Distance between the peaks in the atom density profile of phosphate groups. [f] *xy*-Plane area of the simulation box by the number of lipids per leaflet.

TABLE 13: DOPC Bilayer Structural Parameters from MD Simulations and Their Experimentally Derived Values

	DOPC at 303K		
	experiment[a]	43A1-S3	Berger[b]
V_L (Å^3)	1303	1291	1343
D_B (Å)	38.7	39.1	40.5
D_{HH} (Å)	36.7	36.6[c] (38.1)[d]	37.2[c] (39.8)[d]
$2D_C$ (Å)	28.8	29.0	29.1
A (Å^2)	67.4	66.0	66.3
A_G (Å^2)[e]		65.8	65.4

[a] Values taken from Table 3 of ref 43, fourth column. [b] Values calculated in this work. MD simulations were carried out using the LJ parameters for lipid of Berger et al.[2] and the lipid charge set of Chiu et al.[3] [b] Values calculated in this work. MD simulations were carried out using the Lennard-Jones parameters for lipid of Berger et al.[2] and the lipid charge set of Chiu et al.[3] Lipid topology, coordinate, and parameter files were downloaded from ref 49. [c] Distance between the peaks in the total electron density profile. [d] Distance between the peaks in the atom density profile of phosphate groups. [e] *xy*-Plane area of the simulation box by the number of lipids per leaflet.

reasons mentioned above in the context of cyclohexane, in order to avoid implicit double counting of 1−4 interactions in six-membered rings, KW_{14} type (or RB_{14} type) torsional parameters were used instead of the corresponding equivalent KW type (RB type) ones, which have built-in 1−4 interactions. The VDW_{14} parameters for CHR6 were taken from those for C*H1 (unsaturated methine groups in *n*-alkenes.) The normal 6−12 VDW parameters for CHR6 were then parametrized by MD simulations to reproduce the observed density and ΔH_{vap} of *c*-hexene. (Note that the VDW for

CH2R6 had already been determined in the context of cyclohexane described above; this result is also applied to *c*-hexene.)

2.4.5. Cyclohexanol. Cyclohexanol was employed as a model molecule for obtaining parameters for the hydroxyl group of cholesterol. Atom types for these molecular species were taken from the parameter set 43A1-S3. Standard atom types OA and H from the GROMOS96 parameter set 43A1 were assigned to the hyroxyl oxygen and hydrogen. Bonding parameters for these model molecules were taken from the 43A1-S3 and GROMOS96 43A1 parameter sets. Zero charge was assigned to individual CH2R6 (c-hexanol) atoms. Charges on the COH fragment of *c*-hexanol were scaled manually such that MD simulations reproduced the observed density and ΔH_{vap} of the solvent. The resulting partial charges for the COH group are 0.27 for C, −0.675 for O, and 0.405 for H.

van der Waals Parameters Involving Polar and Charged Atoms. We note that for van der Waals interactions involving charged or polar atoms, the van der Waals parameters for those atoms will be different according to whether the partner atom is nonpolar, polar, or oppositely charged. Table 3A shows the relevant parameters for groups in PC lipids. The numbers in the rows where the atom types are designated by a * are newly computed for the 43A1-S3 force field. The italic numbers show the values carried over from the 43A1 force field.

3. Results for Parameters and Comparison with Experiment for Bilayers

In order to test the force field, we have used it to simulate hydrated lipid bilayers of DPPC, DMPC, DOPC, and DLPC. In developing this force field for lipids, water was not involved. The 43A1-S3 parameters for lipids are hence independent of the water model to be used for membrane simulation. Since the force field is based on GROMOS force field rules and bonding parameters, it may be that water models SPC[45] and SPCE[20] are more compatible with this lipid force field, but we have not done studies to test this. In all of the bilayer simulations described in this paper, the SPCE water model was used.

Fluid-phase bilayers of 100 DMPC and DPPC lipid molecules and 128 DOPC molecules, taken from our earlier membrane simulations,[3,4,47] were used as starting configurations. A bilayer of DLPC was constructed by the following process. An equilibrated DMPC bilayer was converted into a DLPC bilayer by removing two hydrocarbon atoms from the end of each hydrocarbon chain and converting the last methylene group to a methyl group. The initial gap thus created between the two leaflets was eliminated by gradually translocating one leaflet to the other followed by energy minimization of the system. The DOPC bilayer was hydrated with 128 waters per lipid, and each saturated lipid system was hydrated with 32 waters per lipid and equilibrated for 10 ns followed by a production MD run of 50 ns. The MD runs were carried out at 323 K for the DPPC bilayer and 303 K for the DOPC, DLPC, and DMPC bilayers. The particle mesh Ewald method[50] was used for the long-range electrostatic corrections. We used a cutoff of 1.0 nm in the direct space and a Fourier spacing of 0.15 nm. A sixth-order interpolation was applied to the Ewald mesh. For the van der Waals interactions, a twin-range cutoff (1.0/1.6 nm) was applied. The bilayer systems were run under the NPT condition with semi-isotropic pressure coupling (isotropic in the bilayer lateral plane but different along the bilayer normal). The neighbor pair list was updated for every five time steps. All bond lengths of the lipids were constrained with the LINCS algorithm.[8] The SETTLE algorithm[34] was applied to water molecules for bond length constraint. Temperature boundary conditions were set using the Nose−Hoover algorithm.[35] Pressure boundary conditions were set using the Parrinello−Rahman pressure coupling method.[16] In all cases, the SPCE[20] water model was used.

Molecular dynamics simulations of DLPC, DMPC, and DPPC bilayers using GROMOS 43A1,[22] GROMOS 53A6,[40] and Berger[2] force fields were done for comparison, and the monounsaturated bilayer (DOPC) was also simulated with the Berger force field.[2] In general, the simulation conditions used for these comparisons replicated the conditions used by the workers who created those force fields. In particular, the DOPC parameters were based on the Berger force field, and the parameters for the unsaturated carbons were taken from the GROMOS force field.[48] The DOPC parameters and coordinate files can be downloaded from http://bioinf-www.bioinf.uni-sb.de.[49] They were used by us to make the comparison. The lipid charge set of Chiu et al.[3] was used in all cases since that has been incorporated in all of the other force fields. The water model SPC[45] was used for bilayers simulated by using Berger force field because this water model was used by Berger et al. (1997) For all other simulations, the SPCE model[20] was used. The particle mesh Ewald method[50] was used for the long-range electrostatic corrections. A cutoff of 1.0 nm in the direct space and a Fourier spacing of 0.12 nm were used. A fourth-order interpolation was applied to the Ewald mesh. A twin-range cutoff (1.0/1.4 nm) for VDW interactions was applied to MD simulations using GROMOS force fields (43A1 and 53A6). A VDW cutoff of 1.0 nm was applied to simulations using the Berger force field. The temperature and pressure controls of Berendsen et al.[51] were used for all of these MD runs. All of the MD simulations were run under NPT conditions with semi-isotropic pressure coupling. The bilayer systems were equilibrated for 10 ns. In each case, the last 20 ns of a production MD run of at least 30 ns were used for data analysis.

Figure 6 shows the order parameters, S_{CD}, for the Sn-2 chain of DPPC from our MD simulations compared with the experimental results of Douliez et al.[6] The calculated values are in good agreement with the observed results. The average value of S_{CD} in the plateau region (from C4 to C8) is 0.208 in our simulation and 0.217 in the experiments of Douliez et al.[6]

Figure 7a−d shows the simulated X-ray form factors for the four bilayer systems DLPC, DMPC, DPPC, and DOPC and compares them with published experimental values.[11,24,25] As can be seen there, the 43A1 lipid force field does not give calculated form factors comparable to the experimental data. Regarding bilayer structural properties, the 53A6 alkane force field,[40] as well as the 43A1-S3 (this work) force field, gives calculated molecular volumes and heats of vaporization of liquid *n*-alkanes in excellent agreement with experimental data, as can be seen from Figure 2a and b. In addition, the former force field has improved nonbonding parameters for polar atoms based on the free enthalpy of hydration and solvation;[40] yet, it gives too small of an area per lipid, ∼7 Å^2 per lipid smaller than the experimental values, for DLPC, DMPC, and DPPC bilayers (Tables 10−12) when the lipid charge set of Chiu et al.[3] is used. These bilayer systems went into gel phases with an area of 42−44 Å^2 per lipid when the GROMOS lipid charge set[40] of the 53A6 force field was used for simulations.

The form factors (eq A10 in Appendix) calculated for DLPC, DMPC, DPPC, and DOPC bilayers by using the 43A1-S3 force field are in better agreement with experiments than any other force field used in this work (Figure 7a−d). We have already published the corresponding figures for DOPC and POPC.[15] The structural bilayer parameters such as area per lipid (*A*), volume

per lipid (V_L), membrane thickness or Luzzati thickness[14] (D_B), distance between head groups (D_{HH}), and hydrophobic thickness ($2D_C$) predicted by the 43A1-S3 force field are in good agreement with experiments. (Tables 10 and 11). Definitions of these structural parameters and mathematical equations for evaluating their values are from Nagle and Tristram−Nagle[14] and Kucerka et al.[43] We summarize the method of computing these bilayer parameters from MD trajectories in the Appendix.

The quality of the fits provides independent validation of the 43A1-S3 force field since no information about the bilayer structures was used in constructing the force fields or in setting the conditions of the simulation.

4. Summary

We have described the development of new force field parameters (43A1-S3) for united atom MD simulation of lipid membranes. The parameters have been developed from the ground up, by completely reparameterizing force fields for smaller molecules that are components of phospholipid membranes. In particular, we have developed new force fields for hydrocarbons in straight chain, branched, and cyclic configurations and for a variety of organic compounds, shown in Figure 4. The ultimate validation of the work is to show that the force fields for the hydrocarbons and the smaller organic compounds are completely transferable to simulation of phospholipid bilayers, as evidenced by the recreation of X-ray form factors and membrane structures with a high degree of fidelity.

The 43A1-S3 parameters are designed to fit seamlessly into the Gromac simulation package. The full 43A1-S3 force field is provided as Supporting Information to this paper and also may be downloaded from the Nanomedicine Center (http://www.nanoconductor.org/43A1-S3). We request that this paper be cited when the 43A1-S3 force field is used.

Acknowledgment. This work was supported by NIH Grant 5PN2EY016570-05 and by a grant of supercomputing time from the NSF Teragrid. The authors thank Prof. J. F. Nagle for supplying form factor data used in Figure 7.

Appendix

Calculation of Bilayer Structure. The volume per lipid is volumetrically calculated from the following relation

$$V_{box} = N_L V_L + N_W V_W \tag{A1}$$

where V_{box} is volume of the simulation box, N_L and N_W are the numbers of lipids and waters, respectively, in the simulation box, and V_W is the specific volume of the water model used. It can be computed by a separate MD simulation of pure water. Our calculated V_W for SPC are 30.4 Å^3 at 298 K and 31.6 Å^3 at 323 K, and those for SPCE water are 30.0 Å^3 at 298 K and 30.5 Å^3 at 323 K.

The so-defined Luzzati thickness[14] is calculated from

$$D_B = D - \int_{-D/2}^{D/2} P_W(z)\mathrm{d}z \tag{A2}$$

where D is the repeat z-spacing (along the bilayer normal) of the simulation box, $P_W(z)$ is the probability distribution of water along z, and $P_W(z) = 1$ beyond D. $P_W(z)$ is computed from the time-averaged histograms of the water distribution along the z-axis, which is divided into equally spaced bins. Let V_{bin} be the time-averaged volume of each slice with thickness dz, then

$$P_W(z) = N_W(z)V_W/V_{bin} \tag{A3}$$

where $N_W(z)$ is the time-averaged number of water at position z.

Similarily, the hydrobic core thickness is derived from the relation

$$2D_C = \int_{-D/2}^{D/2} P_{HC}(z)\mathrm{d}z \tag{A4}$$

where $P_{HC}(z) = P_{CH3}(z) + P_{CH2}(z)$ for saturated DLPC, DMPC, and DPPC bilayers and $P_{HC}(z) = P_{CH3}(z) + P_{CH2}(z) + P_{CH}(z)$ for the DOPC bilayer. The volume probability distributions CH3, CH2, and CH (unsaturated methine atom) are calculated from

$$P_{CH3}(z) = N_{CH3}(z)V_{CH3}/V_{bin} \tag{A5}$$

$$P_{CH2}(z) = N_{CH2}(z)V_{CH2}/V_{bin} \tag{A6}$$

$$P_{CH}(z) = N_{CH}(z)2V_{CH3}/V_{bin} \tag{A7}$$

histograms of each atom type

Specific volumes for the methyl (V_{CH3}) and methylene (V_{CH2}) groups can be obtained from plotting the alkane specific volume V_{alkane} versus the number of CH2 groups in alkane n as shown

$$V_{alkane} = a + bn \tag{A8}$$

in Figure 2a

The intercept on the y-axis a gives $2V_{CH3}$, and the slope of the plot b corresponds to V_{CH2}. Assuming that the specific volume of 5-*cis*-decene is made up of $2V_{CH3}$, $6V_{CH2}$, and $V_{CH=CH}$, one can estimate that $V_{CH} = V_{CH=CH}/2$. Table A1 summarizes our simulations results for different force fields.

The area per lipid can be calculated[43] using the relation

$$A = 2V_L/D_B \tag{A9}$$

Dividing the xy-plane area of the simulation box by the number of lipids per leaflet gives the surface area per lipid commonly cited in the literature. We label it as A_G in Tables 10−13.

TABLE A1: Specific Volumes for CH3, CH2, CH=CH

	experiment	43A1-S3		53A6		Berger	
	298 K	298 K	323 K	298 K	323 K	298 K	323 K
V_{CH3} (Å^3)	55.2	54.3	57.4	54.2	57.3	68.5	86.8
V_{CH2} (Å^3)	26.9	27.1	27.3	27.2	27.4	25.2	26.2
$V_{CH=CH}$ (Å^3)		44.4					

Bilayer form factors derived from MD simulations are obtained from the Fourier transform[14,43]

$$F(q) = \int_{-D/2}^{D/2} (\rho_{\text{lipid}}(z) - \rho_{\text{water}}) \cos(qz) \mathrm{d}z \quad \text{(A10)}$$

where $\rho_{\text{lipid}}(z)$ is the electron density of a single bilayer at position z and ρ_{water} is the electron density of bulk water.

Supporting Information Available: Bonding and nonbonding parameters. This material is available free of charge via the Internet at http://pubs.acs.org.

References and Notes

(1) Berendsen, H. J. C.; van der Spoel, D.; van Drunen, R. Gromacs: A message-passing parallel molecular dynamics implementation. *Comput. Phys. Commun.* **1995**, *91*, 43–56.

(2) Berger, O.; Edholm, O.; Jähnig, F. Molecular dynamics simulations of a fluid bilayer of dipalmitoylphosphatidylcholine at full hydration, constant pressure, and constant temperature. *Biophys. J.* **1997**, *72*, 2002–2013.

(3) Chiu, S.-W.; Clark, M.; Subramaniam, S.; Scott, H. L.; Jakobsson, E. Incorporation of surface tension into molecular dynamics simulation of an interface: A fluid phase lipid bilayer membrane. *Biophys. J.* **1995**, *69*, 1230–1245.

(4) Chiu, S.-W.; Clark, M. M.; Jakobsson, E.; Subramaniam, S.; Scott, H. L. Optimization of hydrocarbon chain interaction parameters: Application to the simulation of fluid phase lipid bilayers. *J. Phys. Chem. B* **1999**, *103*, 6323–6327.

(5) Chiu, S.-W.; Vasudevan, S.; Jakobsson, E.; Mashl, R. J.; Scott, H. L. Structure of sphingomyelin bilayers: A simulation study. *Biophys. J.* **2003**, *85*, 3624–3635.

(6) Douliez, J.-P.; L'onard, A.; Dufourc, E. J. Restatement of order parameters in biomembranes: Calculation of C−C bond order parameters for C−D quadrupolar splittings. *Biophys. J.* **1995**, *68*, 1727–1739.

(7) Edholm, O.; Nagle, J. F. Areas of molecules in membranes consisting of mixtures. *Biophys. J.* **2005**, *89*, 1827–1832.

(8) Hess, B.; Bekker, H.; Berendsen, H. J. C.; Fraaige, J. G. E. M. LINCS: A linear constraint solver for molecular simulations. *J. Comput. Chem.* **1997**, *18*, 1463–1472.

(9) Japan Chemistry Program Exchange. Proceedings of the 4th Symposium on Computational Chemistry; Tokyo, Japan, 1994.

(10) Klauda, J. B.; Kucerka, N.; Brooks, B. R.; Pastor, R. W.; Nagle, J. F. Simulation-based methods for interpreting X-ray data from lipid bilayers. *Biophys. J.* **2006**, *90*, 2796–2807.

(11) Kucerka, N.; Tristram-Nagle, S.; Nagle, J. F. Structure of fully hydrated fluid phase lipid bilayers with monounsaturated chains. *J. Membr. Biol.* **2005**, *208*, 193–202.

(12) Lindahl, E.; Hess, B.; van der Spoel, D. Gromacs 3.0: A package for molecular simulation and trajectory analysis. *J. Mol. Model.* **2001**, *7*, 306–317.

(13) Nagle, J. F.; Tristram-Nagle, S. Lipid bilayer structure. *Curr. Opin. Struct. Biol.* **2000**, *10*, 474–480.

(14) Nagle, J. F.; Tristram-Nagle, S. Structure of lipid bilayers. *Biochim. Biophys. Acta* **2000**, *1469*, 159–195.

(15) Pandit, S. A.; Chiu, S.-W.; Jakobsson, E.; Grama, A.; Scott, H. L. Cholesterol packing around lipids with saturated and unsaturated chains: A simulation study. *Langmuir* **2008**, *24*, 6858–6865.

(16) Parrinello, M.; Rahman, A. Polymorphic transitions in single crystals: A new molecular dynamics method. *J. Appl. Phys.* **1981**, *52*, 182–7190.

(17) Reiling, M.; and Schlenkrich, S.; Brickmann, J. Force field parameters for carbohydrates. *J. Comput. Chem.* **1996**, *17*, 450–468.

(18) Ryckaert, A.; Bellemans, J. P. Molecular dynamics of liquid alkanes. *Faraday Discuss. Chem. Soc.* **1978**.

(19) Smondyrev, A. M.; Berkowitz, M. L. Structure of dipalmitoylphosphatidylcholine/cholesterol bilayer at low and high cholesterol concentrations: Molecular dynamics simulation. *Biophys. J.* **1999**, *77*, 2075–2089.

(20) Berendsen, H. J. C.; Grigera, J. R.; Straatsma, T. P. The missing term in effective pair potentials. *J. Phys. Chem.* **1987**, *91*, 6269–6271.

(21) Tobias, D. J.; Tu, K.; Klein, M. L. Atomic-scale molecular dynamics simulations of lipid membranes. *Curr. Opin. Colloid Interface Sci.* **1997**, *2*, 15–26.

(22) van Gunsteren, W. F. Billeter, S. R. Eising, R. A. Hünenberger, P. H. Krüger, P. Mark, A. E. Scott, W. R. P.; Tironi. I. G. Biomolecular Simulation: The GROMOS96 Manual and User Guide; Hochschulverlat van der ETH Zurich/Biomos: Zurich, Groningen, The Netherlands, 1996.

(23) Zhang, L.; McQuaw, C. M.; Ewing, A. G.; Winograd, N. Sphingomyelin/phosphatidylcholine and cholesterol interactions studied by imaging mass spectromitry. *J. Am. Chem. Soc.* **2007**, *129*, 15730–15731.

(24) Kucerka, N.; Liu, Y.; Chu, N.; Petrache, H. I.; Tristram-Nagle, S.; Nagle, J. F. Structure of fully hydrated fluid phase DMPC and DLPC lipid bilayers using X-ray scattering from oriented multilamellar arrays and from unilamellar vesicles. *Biophys. J.* **2005**, *88*, 2626–2637.

(25) Kucerka, N.; Tristram-Nagle, S.; Nagle, J. F. Closer look at structure of fully hydrated fluid phase DPPC bilayers. *Biophys. J.* **2006**, *90*, L83−85L.

(26) Ryckaert, J.-P.; Ciccotti, G.; Berendsen, J. J. C. Numerical integration of the cartesian equations of motion of a system with constraints: molecular dynamics of n-alkanes. *J. Comput. Phys.* **1977**, *23*, 327–341.

(27) Frisch, M. J.; Trucks, G. W.; Schlegel, H. B.; Scuseria, G. E.; Robb, M. A.; Cheeseman, J. R.; Montgomery, J. A., Jr.; Vreven, T.; Kudin, K. N.; Burant, J. C.; Millam, J. M.; Iyengar, S. S.; Tomasi, J.; Barone, V.; Mennucci, B.; Cossi, M.; Scalmani, G.; Rega, N.; Petersson, G. A.; Nakatsuji, H.; Hada, M.; Ehara, M.; Toyota, K.; Fukuda, R.; Hasegawa, J.; Ishida, M.; Nakajima, T.; Honda, Y.; Kitao, O.; Nakai, H.; Klene, M.; Li, X.; Knox, J. E.; Hratchian, H. P.; Cross, J. B.; Bakken, V.; Adamo, C.; Jaramillo, J.; Gomperts, R.; Stratmann, R. E.; Yazyev, O.; Austin, A. J.; Cammi, R.; Pomelli, C.; Ochterski, J. W.; Ayala, P. Y.; Morokuma, K.; Voth, G. A.; Salvador, P.; Dannenberg, J. J.; Zakrzewski, V. G.; Dapprich, S.; Daniels, A. D.; Strain, M. C.; Farkas, O.; Malick, D. K.; Rabuck, A. D.; Raghavachari, K.; Foresman, J. B.; Ortiz, J. V.; Cui, Q.; Baboul, A. G.; Clifford, S.; Cioslowski, J.; Stefanov, B. B.; Liu, G.; Liashenko, A.; Piskorz, P.; Komaromi, I.; Martin, R. L.; Fox, D. J.; Keith, T.; Al-Laham, M. A.; Peng, C. Y.; Nanayakkara, A.; Challacombe, M.; Gill, P. M. W.; Johnson, B.; Chen, W.; Wong, M. W.; Gonzalez, C.; Pople, J. A. *Gaussian 03*, revision C.02; Gaussian, Inc.: Wallingford, CT, 2004.

(28) Smith, G. D.; Paul, W. United atom force field for molecular dynamics simulations of 1,4-polybutadiene based on quantum chemistry calculations on model molecules. *J. Phys. Chem. A* **1998**, *102*, 1200–1208.

(29) Chandrasekhar, I.; Kastenholz, M.; Lins, R. D.; Oostenbrink, C.; Schuler, L. D.; Tieleman, D. P.; van Gunsteren, W. F. A consistent potential energy parameter set for lipids: dipalmitoylphosphatidylcholine as a benchmark of the GROMOS96 45A3 force field. *Eur. Biophys. J.* **2003**, *32*, 67–77.

(30) Florian, J. Conformational flexibility of phosphate, phosphonate, and phosphorothioate methyl esters in aqueous solution. *J. Am. Chem. Soc.* **1998**, *120*, 7959–7966.

(31) Alber, F.; Carloni, P. Dimethyl phosphate: Stereoelectronic versus environmental effects. *J. Phys. Chem. B* **1999**, *103*, 6121–6126.

(32) Leulliot, N.; Scalamani, G. Ground state properties of the nucleic acid constituents studied by density functional calculations. I. Conformational features of ribose, dimethyl phosphate, uridine, cytidine, 5′-methyl phosphate-uridine, and 3′-methyl phosphate-uridine. *J. Phys. Chem. A* **1999**, *103*, 8716–8724.

(33) Banavali, N. K.; MacKerell, A. D., Jr. Reevaluation of stereoelectronic contributions to the conformational properties of the phosphodiester and N3′-phosphoramidate moieties of nucleic acids. *J. Am. Chem. Soc.* **2001**, *123*, 6747–6755.

(34) Miyamoto, S; Kollman, P. A. SETTLE: An analytical version of the SHAKE and RATTLE algorithm for rigid water models. *J. Comput. Chem.* **1992**, *13*, 952–962.

(35) Evans, D. J.; Holian, B. I. The Nose−Hoover thermostat. *J. Chem. Phys.* **1985**, *83*, 4069.

(36) Lide, D. R., Ed. *CRC Handbook of Chemistry and Physics*, 86th edition; CRC Press: Boca Raton, FL,2005.

(37) Jorgensen, W. L.; Madura, J. D.; Swenson, C. J. Optimized intermolecular potential functions for liquid hydrocarbons. *J. Am. Chem. Soc.* **1984**, *106*, 6638–6646.

(38) Martin, M. G.; Siepmann, J. I. Transferable potentials for phase equilibria. 1. United-atom description of n-alkanes. *J. Phys. Chem. B* **1998**, *102*, 2569–2577.

(39) Nath, S. K.; Escobedo, F. A.; de Pablo, J. J. On the simulation of vapor−liquid equilibria for alkanes. *J. Chem. Phys.* **1998**, *108*, 9905–9911.

(40) Oostenbrink, C.; Villa, A.; Mark, A. E.; van Gunsteren, W. F. A biomolecular force field based on the free enthalpy of hydration and solvation: The GROMOS force-field parameter sets 53A5 and 53A6. *J. Comput. Chem.* **2004**, *25*, 1656–1676.

(41) Schuler, L. D.; Daura, X.; van Gunsteren, W. F. An improved GROMOS96 force field for aliphatic hydrocarbons in the condensed phase. *J. Comput. Chem.* **2001**, *22*, 1205–1218.

(42) Kucerka, N.; Liu, Y.; Chu, N.; Petrache, H. I.; Tristram-Nagle, S.; Nagle, J. F. Structure of fully hydrated fluid phase DMPC and DLPC bilayers using X-ray scattering from oriented multilamellar arrays and from unilamellar vesicles. *Biophys. J.* **2005**, *88*, 2626–2637.

(43) Kucerka, N.; Nagle, J. F.; Sachs, J. N.; Feller, S. E.; Pencer, J.; Jackson, A.; Katsaras, J. Lipid bilayer structure determined by the simultaneous analysis of neutron and X-ray scattering data. *Biophys. J.* **2008**, *95*, 2356–2367.

(44) Hermans, J.; Berendsen, H. J. C.; van Gunsteren, W. F.; Postma, J. P. M. *Biopolymers* **1984**, *23*, 1513.

(45) Berendsen, H. J. C.; Postma, J. P. M.; van Gunsteren W. F.; Hermans, J. In *Intermolecular Forces*; Pullman, B., Ed.; Reidel: Dordrecht, The Netherlands, 1981; p 331.

(46) Mulliken, R. S. Electronic population analysis on LCAO-MO molecular wave functions. I. *J. Chem. Phys.* **1955**, *23*, 1833–1840.

(47) Chiu, S. W.; Jakobsson, E.; Subramaniam, S.; Scott, H. L. Combined Monte Carlo and molecular dynamics simulation of fully hydrated dioleyl and palmitoyl-oleyl phosphatidylcholine lipid bilayers. *Biophys. J.* **1999**, *77*, 2462–2469.

(48) Siu, S. W. I.; Vácha, R.; Jungwirth, P.; Böckmann, R. A. Biomolecular simulations of membranes: Physical properties from different force fields. *J. Chem. Phys.* **2008**, *128*, 125103–125112.

(49) Lipid force field topologies and snapshots of equilibrated structures. http://www.bioinf.uni-sb.de/RB/download.html(accessed on Nov. 24, 2008).

(50) Darden, T.; York, D.; Pederson, L. Particle mesh Ewald: An W log(*N*) method for Ewald sums in large systems. *J. Chem. Phys.* **1993**, *98*, 10089–10092.

(51) Berendsen, H. J. C.; Postma, J. P. M.; van Gunsteren, W. F.; DiNola, A.; Haak, J. R. Molecular dynamics with coupling to an external bath. *J. Chem. Phys.* **1984**, *81*, 3684–3690.

JP807056C